A heuristic method to identify runs of homozygosity associated with reduced performance in livestock

J. T. Howard*, F. Tiezzi*, Y. Huang†, K. A. Gray†, C. Maltecca*‡

*Department of Animal Science, North Carolina State University, Raleigh, NC 27695-7627, USA.

†Smithfield Premium Genetics, Rose Hill, NC 28458, USA

‡Genetics Program, North Carolina State University, Raleigh, NC 27695-7627, USA.

Corresponding Author: Jeremy Howard

Address: Department of Animal Science

North Carolina State University,

Raleigh, NC 27695-7627

Phone: (919) 515-0811

E-mail: jthoward@ncsu.edu

ABSTRACT

While for the most part genome-wide metrics are currently employed in managing livestock inbreeding, genomic data offer, in principle, the ability to identify functional inbreeding. Here we present a heuristic method to identify haplotypes contained within a run of homozygosity (ROH) associated with reduced performance. Results are presented for simulated and swine data. The algorithm comprises 3 steps. Step 1 scans the genome based on marker windows of decreasing size and identifies ROH genotypes associated with an unfavorable phenotype. Within this stage, multiple aggregation steps reduce the haplotype to the smallest possible length. In step 2, the resulting regions are formally tested for significance with the use of a linear mixed model. Lastly, step 3 removes nested windows. The effect of the unfavorable haplotypes identified and their associated haplotype probabilities for a progeny of a given mating pair or an individual can be used to generate an inbreeding load matrix (**ILM**). Diagonals of **ILM** characterize the functional inbreeding load of individual (IIL). We estimated the accuracy of predicting the phenotype based on ILL. We further compared the significance of the regression coefficient for IIL on phenotypes to genome-wide inbreeding metrics. We tested the algorithm using simulated scenarios (n =12) combining different levels of linkage disequilibrium (LD) and number of loci impacting a quantitative trait. Additionally, we investigated 9 traits from two maternal purebred swine lines. In simulated data, as the LD in the population increased the algorithm identified a greater proportion of the true unfavorable ROH effects. For example, the proportion of highly unfavorable true ROH effects identified raised from 32 to 41 % for the low to the high LD scenario. In both simulated and real data the haplotypes identified were contained within a much larger

ROH (9.12-12.1 Mb). The IIL prediction accuracy was greater than zero across all scenarios for simulated data (high LD scenario mean (95% confidence interval): 0.49 (0.47-0.52)) and for nearly all swine traits (mean ± SD: 0.17±0.10). On average across simulated and swine datasets the IIL regression coefficient was more closely related to progeny performance than any genome-wide inbreeding metric. A heuristic method was developed that identified ROH genotypes with reduced performance and characterized the combined effects of ROH genotypes within and across individuals.

Key Words: inbreeding, runs-of-homozygosity, swine.

INTRODUCTION

The implementation of routine genotyping within livestock breeding populations has become a common practice and is used as a tool to make more effective selection decisions in swine breeding companies (Knol et al., 2016). Previous research has highlighted the advantages of genomic relationships compared to pedigree-based information to obtain more precise estimates of the genetic merit and homozygosity of an individual (Knol et al., 2016; Lopes et al., 2013). Also, genomic information allows genome-wide inbreeding estimates to be supplemented by characterizing the impact of homozygosity for specific genomic regions. Elevated levels of homozygosity result in a reduction in phenotypic performance, referred to as inbreeding depression (Falconer and Mackay, 1996). The identification of region-specific stretches allows breeders to manage inbreeding more effectively since the impact of homozygosity for a trait can vary across the genome. The estimation of dominance effects to identify unfavorable regions of the genome have been utilized in the past (Lopes et al., 2016; Xiang et al., 2016), but lacks power for low frequency mutations and doesn't consider that whole segments of the

genome are passed from parent to offspring. To overcome these limitations, regions of the genome in a continuous run of homozygosity (ROH) have been proposed to investigate homozygous segments that arose due to past inbreeding (Howard et al., 2015; Saura et al., 2015). Previous research has investigated the phenotypic effect of a region being in an ROH (Pryce et al., 2014; Howard et al., 2015). The previous methods did not directly identify the unique ROH genotype that gave rise to the reduced phenotypic performance. Within this paper, we have attempted to close this gap by developing a heuristic algorithm to identify unfavorable haplotypes contained within ROH across the genome. The method was tested on simulated as well as real data.

MATERIALS AND METHODS

No animal care approval was required for this work since all genotypes and records came from data that were available from previous studies. The manuscript will be split in two sections. In the first section, we will provide an overview of the algorithm along with methods to summarize the number of unfavorable haplotypes shared within and across individuals. In the second part of the paper we will employ simulated and swine data sets to summarize three major results: (1) how effective the algorithm is at identifying unfavorable haplotypes, (2) the length of ROH the unfavorable haplotype tags, (3) the relationship of the aggregate effect of unfavorable haplotypes carried by an individual with its phenotype and genetic value.

Description of the algorithm

A pictorial overview of the algorithm is displayed in **Figure 1**. The method follows three steps. The first step scans the genome to identify ROH genotypes that result in an unfavorable change in the phenotype of interest. The genotypes utilized in the

algorithm are coded as 0 for the homozygote, 2 for the alternative homozygote and 1 for the heterozygote. Step 1 begins at the first SNP of a chromosome by constructing a window of a predetermined number of SNP (default = 60). Within a window, the mean phenotype is tabulated for each unique ROH genotype and any genotype that is not in a ROH is aggregated into a category referred to as nonROH. Furthermore, any ROH genotype below a user defined frequency (default = 0.0075) is removed from the ROH genotype list and placed in the nonROH category. If the phenotypic mean for a ROH genotype is below/above a user defined value (discussed below), the window is stored. Next, the window is shifted forward by one SNP and the previous process is repeated. Once the entire chromosome has been scanned, windows containing the same set of animals and representing the same ROH genotype except for the first and last SNP are aggregated (i.e. **Figure 1**: Step 1b). Since recombination does not occur within a given region for the individuals of the same ROH genotype, ROH genotypes that are combined in this step contain the same amount of information. Following the aggregation of nested windows, the window length is reduced by "n" SNP (default = 5) and the previous steps are repeated for the new window size. The window size is reduced by "n" until a minimum window size is reached (default = 20). Once the minimum window size is reached, the process of scanning for unfavorable ROH genotypes is complete for a chromosome. For windows that contain the same set of animals and are nested within each other (i.e. **Figure 1**: Step 1d), the shortest window is kept for further analysis. The aggregation steps (i.e. Step 1b and 1d) trap the ROH genotypes across individuals that have the same core ROH genotype of the smallest possible length. No information is lost within the aggregation steps as each ROH genotype belongs to the same set of

individuals, yet the step significantly reduces the number of windows tested in following steps. The core ROH genotype is now expected to serve as a tag for the full ROH segment observed in an individual, which may differ across subjects due to recombination occurring at different locations across subjects.

Any window remaining after Step 1 is subsequenly tested for significance using a standard mixed model that accounts for the environment, additive genetic and permanent environment effect of an individual, plus any number of fixed effects. A description of the full model for each window is outlined below:

$$y = \boldsymbol{X}b + \boldsymbol{Z}a + \boldsymbol{W}pe + e,$$

where *y* is the trait of interest, *b* is a vector of fixed effects, *a* is a vector of random additive genetic effects, *pe* is a vector of random permanent environmental effects, *e* is a vector of random residuals and **X**, **Z**, and **W** are incidence matrices relating *b*, *a* and *pe* with *y*, respectively. The fixed effects can include any environmental classification or covariate effect along with the effect of ROH genotype (i.e. unique ROH genotype and nonROH) for a given window. The random additive genetic effect is assumed ~N(0, $\mathbf{A}\sigma_a^2$), with **A** representing the additive relationship matrix derived from a pedigree (Henderson, 1976). The random permanent environmental and residual effects are assumed ~N(0, $\mathbf{I}\sigma_{pe}^2$) and ~N(0, $\mathbf{I}\sigma_e^2$), respectively, with **I** being an identity matrix. Variance components of the current implementation are assumed fixed across windows based on the null model of no ROH effect (i.e. no ROH genotype in the model). For each window, solutions are obtained via the Cholesky decomposition of the left-hand side (**LHS**). Given the solutions for each window, a contrast between each unique ROH genotype versus nonROH and the associated t-statistic are obtained. The contrasts ($\mathbf{L}\hat{\beta}$)

are obtained following Welham et al. (2004) and Gilmour et al. (2004). The t-statistic is generated based on the following formula:

$$t_{(\mathrm{L}\hat{\beta})} = \frac{L\hat{\beta}-0}{\sigma_{L\hat{\beta}}},$$

where $\mathbf{L}\hat{\beta}$ refers to the estimated contrast and $\sigma_{L\hat{\beta}}$ refers to the standard error of the contrast, calculated as $\mathbf{L(LHS^{-1})L'}$. The hypothesis test is one-sided and the direction of the test is dependent on the direction of the unfavorable phenotype. Under this parameterization, the genotypes not in an ROH are assumed normal compared to individuals that have the ROH genotype. This aligns with the partial dominance hypothesis, which is thought to account for the majority of inbreeding depression observed in populations (Simmons and Crow, 1977; Charlesworth and Charlesworth, 1987). Any contrast that passes the user-defined significance threshold is kept and moved onto the final window reduction step which resolves nested windows (i.e. **Figure 1**: Step 3).

The algorithm presented was developed in C++11. The source code and compiled executable files for Linux operating systems are available at "https://github.com/jeremyhoward". The primary option the user controls is the cutoff value for the mean phenotype for a given ROH genotype that is considered unfavorable in Step1a. The user can specify a cutoff value based on prior knowledge of what is considered an unfavorable phenotype or generate an empirical t-statistic distribution from the data to declare a cutoff value. The latter option is conducted by randomly specifying a chromosome, window length and start position and estimating the significance value for ROH genotypes within the window. All one-sided t-statistics are stored. Across samples,

the mean phenotype for t-statistics with a significance ranging from 0.10 and 0.05 is chosen as the cutoff value.

The haplotypes identified can be utilized in a variety of ways, but two are investigated in the current study. The first application is to apply the algorithm across economically important phenotypes and identify haplotypes having an unfavorable effect across multiple traits. Regions with consistent unfavorable effect across multiple traits should have a high probability of being sensitive to inbreeding and thus result in a reduction in the overall fitness and vigor of an individual. The second application is to generate a matrix aiming at characterizing the decrease in the trait of interest across all unfavorable haplotypes, herein referred to as the inbreeding load matrix (**ILM**). Its calculation follows the method outlined by Cole (2015). In order to implement an **ILM**, the genotype phase needs to be known. This matrix then can be utilized in mating designs to minimize the probability of progeny containing the unfavorable haplotype(s) for a single trait or across multiple traits. The diagonals of the matrix, referred to as individual inbreeding load (IIL), represent an individual's decrease in the phenotypic performance(s) due to inbreeding, while off-diagonals represent the decrease in the trait(s) of the progeny given the mating of the two (potential) parents. It should be noted that in this implementation the algorithm does not run all haplotypes across the genome simultaneously. As a result, any observed ROH genotype for an individual might contain multiple significant unfavorable haplotypes. Therefore multiple tag haplotypes identified by the algorithm could be counted as different in an individual, when in fact they are tagging the same observed haplotype. Within the current study, when multiple haplotypes tagged the same observed ROH genotype, only the haplotype with the highest

significance value and resulting in the largest number of haplotypes observed across individuals was retained. For the i^{th} row and j^{th} column of **ILM**, the following formula was utilized to calculate the value:

$$ILM_{ij} = \sum_{h=1}^{h=n} (ROH)_h * \hat{\beta}_h,$$

where *n* is the number of unfavorable haplotypes that remained after eliminating haplotypes that were not observed or removed to avoid double counting. The ROH_h refers to the probability of generating a ROH for haplotype$_h$ and β_h is the effect of the ROH genotype estimated from Step 2 of the algorithm. The probability values for the diagonals elements of the ILM include 0.25 (haplotype carrier) or 1.0 (haplotype in ROH). The probability values for the off-diagonal elements include 0.25 (mating of haplotype carriers), 0.5 (mating of haplotype carrier and ROH genotype) or 1.0 (both parents have ROH genotype). The **ILM** values range from 0 (i.e. no unfavorable haplotypes) to any value in the unfavorable direction.

Summary of metrics utilized to test the algorithm using simulated and swine data

Simulated datasets, where the true genetic signal is known, were employed to determine how effective the algorithm was at identifying true negative ROH regions as well as to characterize the relationship between IIL and the true aggregate genotypic value of individuals. The length of ROH the unfavorable haplotype tagged was determined across both simulated and swine datasets in order to ensure that long stretches of ROH were represented. Long ROH stretches have a higher probability of being true IBD segments as a result of recent inbreeding, compared to shorter ones. The relationship between IIL and the phenotype was summarized based either on a) IIL accuracy of predicting the phenotype or b) the significance of the regression coefficient

when IIL was included as a fixed covariate in a mixed linear model. The latter relationship was generated under the premise that the management of inbreeding is traditionally done by minimizing parental coancestries using genome-wide inbreeding metrics. Therefore, the significance (i.e. *–log p-value*) of the regression coefficient from traditionally utilized genome-wide inbreeding metrics was compared with the IIL value. Lastly, IIL was benchmarked across simulated and swine datasets with estimates of the genetic value based on a whole genome regression model. This was conducted to generate a reference comparison on the prediction accuracy for a given trait based on traditionally utilized genome-wide modeling techniques. It is important to note that the genetic signal from IIL encompasses only unfavorable effects resulting from long IBD segments. As a result, a comparison of the prediction accuracies between the two metrics needs not to be interpreted as an exercise of ranking the predictive ability of the two metrics, (ILL value would by construction only capture a subset of the overall genetic signal) but rather to determine the relationship between complementary metrics, in order to allow their integration.

Simulated Data

Multiple scenarios were simulated to determine the frequency of unfavorable haplotypes being identified by the algorithm. Simulation was carried out using Geno-Diver (Howard et al. In Press), a combined coalescence and forward in time simulation software. We hypothesized that the amount of short-range LD existing in the genome impacts how well the algorithm can identify unfavorable haplotypes. Four scenarios of increasing levels of short-range LD in the historical population were generated as outlined in **Figure S1** and will be referred to as the *low*, *low-medium*, *medium-high* and

229 *high*, respectively. For each LD scenario, different genetic architectures were simulated
230 with 250, 500 or 1000 QTL spread equally across 5 chromosomes. The combination of
231 variable LD and QTL parameters produced 12 different scenarios. Each scenario was
232 replicated 25 times.

233 Within each LD setting, SNP sequence data for 4000 base haplotypes across 5
234 chromosomes, each with a length of 150 Megabases, were simulated by internally calling
235 MaCS (Chen et al., 2009) within the Geno-Diver software. Scenarios with the same LD
236 parameter were initialized using the same set of sequence data to limit the computational
237 time and variability across replicates due to historical sequence information. Following
238 the generation of sequence data, QTL were randomly placed along the genome and a
239 SNP panel with neutral markers was created. A total of 4,000 markers (20,000 genome-
240 wide) were utilized within each chromosome. This marker density was chosen to
241 generate a density within each chromosome that is similar to a medium density marker
242 array such as the Illumina PorcineSNP60K (Illumina Inc., San Diego, CA). Across all
243 scenarios, the minimum minor allele frequency was set at 0.10 and 0.015 for markers and
244 QTL, respectively.

245 For each QTL the additive effect (*a*) of a QTL, defined as half the difference in
246 genotypic value between the homozygote genotypes (Falconer and Mackay, 1996), was
247 sampled from a gamma distribution (shape = 0.4; scale = 1.66) with an equal chance of
248 being positive or negative. The dominance effect (*d*) of a QTL, defined as the deviation
249 of the genotypic value of the heterozygote from the mean of the genotypic values of the
250 two homozygotes (Falconer and Mackay, 1996), was generated similarly to Wellmann &
251 Bennewitz (2012). First, the degree of dominance (*h*) at QTL_i was sampled from a

252 normal distribution (mean = 0.1; variance = 0.04) and then the dominance effect at QTL_i
253 was calculated as $d_i = h_i|a_i|$, where $|a_i|$ is the absolute value of the additive effect. Across
254 all scenarios, the additive and dominance effects were scaled to generate a narrow and
255 broad sense heritability (H^2) of 0.35 and 0.40, respectively. The normal distribution
256 parameters used to generate the degree of dominance were utilized to create a trait that
257 displayed directional dominance along with a majority of the loci displaying partial
258 dominance. Phenotypes were simulated by adding a residual value, generated from a
259 normal distribution (mean = 0, variance = $(1- H^2)$), to the genotypic value for each
260 animal. Summary statistics on the QTL architecture and genetic diversity of the 12
261 scenarios is outlined in **Table S1.**

262 After the founder population and genetic architecture of the trait was generated a
263 selection scenario mimicking a livestock population was undertaken for ten generations.
264 A population consisting of 50 males and 600 females was utilized, with a replacement
265 rate of 20% for both males and females. Progeny with a high estimated breeding value
266 (EBV) were selected to serve as parents for the next generation and EBV were generated
267 from an animal model based on pedigree information. A low phenotypic value
268 represented the unfavorable direction for the simulated trait in this case. Animals were
269 mated at random and one progeny was produced for each mating pair. Progeny born from
270 generation 7 to 9 served as the training population to identify unfavorable haplotypes and
271 progeny from generation 10 served as the validation population. The model utilized to
272 identify unfavorable haplotypes in the simulation data set did not have a permanent
273 environmental effect since individuals only had 1 observation and the only fixed effect
274 was the overall mean. The starting window size was set at 60 and was reduced by 5 until

a window size of 20 SNP was reached. Different SNP window sizes were investigated based on the density simulated. Similar results were found in terms of the regions identified, associated effects and its relationship with the phenotype (data not shown). The suggestive phenotypic cutoff in step 1 was declared by randomly sampling 1000 windows to generate the empirical t-statistic distribution.

To investigate the proportion of true negative ROH effects the algorithm captured within each replicate, the true effect for any ROH with a length greater than 1 Mb was calculated. A length of 1 Mb was chosen to provide a range of possible ROH lengths captured by the algorithm. The true negative and positive ROH effects were split into quantiles of decreasing and increasing effects, respectively. The algorithm only tests for the unfavorable direction and therefore the percentage of true ROH effects the algorithm identified is expected to be higher in the negative compared to the positive direction. Lastly, using the same 1 Mb ROH cutoff, statistics on the length of ROH the algorithm identified (or missed) were calculated.

Within each replicate, the ILL was estimated based on haplotypes identified in the training population for individuals in the validation population. The correlation between IIL and the true genotypic value (TGV), true breeding value (TBV) and true dominance deviation (TDD) was also estimated. Additionally, the significance (i.e. *–log p-value*) of IIL or a genome-wide metric when included as a fixed covariate effect was estimated for the validation population. The ILL or genome-wide metric was included as a fixed covariate in the similar model (i.e. no ROH effect included in model) that was used to identify haplotypes in the training population. Three genome-wide inbreeding metrics were used as comparison including pedigree inbreeding (Henderson, 1976), diagonals of

298 the SNP-by-SNP relationship matrix (**SNPRM**; VanRaden, 2008) or proportion of the
299 markers that were homozygous.

300 To explore the predictive ability of IIL compared to estimates of the genetic value
301 utilizing whole genome regression models, a Bayesian Ridge Regression (BRR) analysis
302 was conducted that included the additive and dominance effect for each SNP. The same
303 training and validation generations that were utilized previously were also used in the
304 BRR analysis. Marker effects were estimated using the 'BGLR' package in R (Perez and
305 de los Campos, 2014). A total of 55,000 iterations were run with the first 5,000 discarded
306 as burn-in and a thinning rate of 5. Across individuals, the estimated breeding value
307 (EBV), dominance deviation (EDD) and genotypic value (EGV) were generated by
308 multiplying the estimated effect by the associated genotype and summing across all
309 markers. The prediction accuracy for either IIL or EGV was determined in the validation
310 population based on the correlation between phenotype and EGV or IIL, respectively. It
311 was standardized by dividing by the square root of the heritability estimated in the
312 training generation for each replicate (Legarra et al., 2008; Wolc et al., 2011).
313 Correlations between IIL and the EBV, EDD or EGV were also estimated.

314 ***Swine Data***

315 Phenotypic and genotypic data from two maternal purebred nucleus selection lines
316 were obtained from Smithfield Premium Genetics (Rose Hill, NC). In order to determine
317 the algorithm's behavior across different genetic architectures, multiple traits were
318 investigated including litter size, litter viability and growth rate. Individuals with
319 genotype information from Large White (LW, n = 6,750) and Landrace (LR, n = 5,010)
320 were utilized. Animals born before 2012 were used as a training population and animals

born on 2013 were used as a validation population and the number of animals across traits is outlined in **Table 1**. A complete description of the genotype quality control is outlined in Howard et al. (2016). Briefly, genotype data was derived from the Illumina PorcineSNP60K BeadChip (Illumina Inc., San Diego, CA) and the GGP-Porcine (GeneSeek Inc., a Neogen Co., Lincoln, NE). Multiple quality control measures were conducted before imputing and phasing missing and low-density to medium-density genotypes using Beagle (Version 3; Browning & Browning 2007). After quality control and discarding SNP that were poorly imputed, a total of 39,671 and 41,489 autosomal SNP for LW and LR remained, respectively.

Seven litter size and mortality traits including number born alive (NBA), total number born (TNB), proportion born dead (PD), average litter birth weight (LBW), preweaning mortality (PWM), number weaned (NW) and average litter wean weight (NWBW) were employed in the analysis. The TNB phenotype included NBA, stillborn and mummified piglets. The PD dead was calculated as 1 - (NBA/TNB). The LBW was calculated as the mean weight of the number of live piglets at processing, which occurred within 48 h from birth. Traits that were recorded after birth, including PWM, NW and NWBW, are impacted by the degree of cross-fostering. Cross-fostering in the current data was similar to previous estimates by Putz et al. (2015) in a related population. To minimize the effect of cross-fostering only litters having more than 75 % of the birth sow piglets were utilized in the analysis. After the data edit, 98.0 and 97.7 % of the piglets were nursed by their original birth sow for LW and LR, respectively. The PWM mortality phenotype was calculated as the number of piglets that died after 24 hours including pigs euthanized at weaning divided by the total number of pigs in the litter after the 24-hour

cutoff. The NWBW was calculated as the average weight of the number of piglets weaned. All reproductive traits were evaluated as a trait of the biological dam. The fixed effects utilized for each trait are outlined in **Table 1.** A random additive genetic and permanent environmental effect of the dam were included in the analysis (i.e. similar to Model 1 described in the section outlining the algorithm).

Two production traits were investigated: body weight at off-test and average body weight gain from birth to off-test (i.e. body weight at off-test / age at off-test). Production traits were evaluated as a trait of the animal. Since animals only have one observation the permanent environmental effect was in this case excluded. The fixed effects utilized for each trait are described in **Table 1**. Across both reproductive and production traits, the contemporary group (CG) was comprised of farm, year and season and any animal that was within a CG smaller than 5 was removed from the analysis.

Summary statistics on the length of ROH and the unfavorable haplotypes captured were generated. Prediction accuracy for IIL was compared with a whole genome regression BRR model. For all 9 traits, yield deviations were constructed for each trait based on the fixed effects outlined in **Table 1**. For the reproductive traits, an animal may have multiple observations and therefore average yield deviations were used and the residuals for a given observation in the BRR analysis was weighted according to Garrick et al. (2009). The formula used to calculate the weight was:

$$\frac{(1-h^2)}{h^2+\frac{1+r^2(l-1)}{l}-h^2},$$

where h^2 refers to the heritability, r^2 refers to the repeatability and l refers to the number of records. The values used for h^2 and r^2 are outlined in **Table 1** across all nine traits. Utilizing 'BGLR' (Perez and de los Campos, 2014), a total of 155,000 iterations were run

with the first 5,000 discarded as burn-in and a thinning rate of 5. Again, for each trait the EGV values were predicted. The accuracy of predicting the phenotype utilizing IIL compared to a whole-genome regression model and the relationship between the two were investigated. The prediction accuracy for either IIL or EGV across the nine traits was determined in the validation population. The prediction accuracy was calculated as the correlation between the EGV or IIL and average yield deviation. It was standardized by dividing the square root of the heritability for each trait. The significance of the ILL or genome-wide regression coefficient was estimated as outlined previously.

Lastly, the correlation between the diagonal and the off-diagonal elements of **ILM** across traits and with pedigree- and genomic-based relationship matrices were estimated. Understanding the correlation between **ILM** across traits is important when **ILM** is used to minimize inbreeding depression across all traits in a breeding objective. Any change in the off-diagonal **ILM** value for one trait should ideally result in a favorable or negligible change in the off-diagonal **ILM** value for other traits. **ILM** was compared to three relationship matrices including pedigree-based (**A;** Henderson, 1976), **SNPRM** and a ROH-based relationship matrix with a 5 Mb cutoff (**ROH5RM**; Howard et al. 2016). To determine the sensitivity of fixing the variance components based on the null model of no ROH effect, the ASReml program (Gilmour et al., 2009), which re-estimates variance components for each window was utilized across breed and traits for the windows that were deemed significant by the algorithm.

RESULTS

Simulated Data

A summary of how effectively the algorithm identified true negative and positive ROH effects across different percentiles is outlined in **Panel 1 of Figure 2**. Since the algorithm only tests for the unfavorable direction, the percentage of true ROH effects the method identifies is expected to be greater than zero in the negative direction and zero in the positive direction. As illustrated in **Panel 1 of Figure 2**, as the true negative unfavorable ROH effect got larger, a greater proportion of unfavorable ROH genotypes was identified by the algorithm. It should be noted that, averaged across all scenarios, the frequency of highly unfavorable ROH effects was small (1.8 %) compared to the total number of true negative ROH effects. The frequency of incorrectly identified positive ROH effects (i.e. false-positives) by the algorithm remained relatively flat across all percentiles and was on average (95% confidence interval (**CI**)) 9.4 (8.7-10.1) percent across all scenarios. As the LD in the population increased and became similar to that of most livestock populations, the algorithm was more effective at identifying unfavorable haplotypes and had a lower false-positive rate. For example, for true ROH effects with the largest negative effect (i.e. less than the 0.05 percentile), the algorithm identified on average (95% CI) 32.1 (28.5-35.7) and 41.2 (36.7-45.9) percent of the total true negative ROH effects across the three QTL scenarios for the low and high LD scenarios, respectively. Conversely, for incorrectly identified true ROH effects (i.e. estimated to be negative, but had a true positive effect) with the largest positive effect (i.e. greater than the .95 percentile), the algorithm identified on average (95% CI) 15.3 (13.9-16.7) and 9.6 (8.2-10.9) percent of the total true ROH effects across the three QTL scenarios for the low and high LD scenario, respectively.

411 Summary statistics on the length of ROH of at least 1 Mb tagged by the
412 unfavorable haplotype is outlined in **Panel 2 of Figure 2**. We report the median in this
413 case, rather the mean, since the distribution of the length of ROH containing a tag
414 haplotype has a heavy tail and thus the latter parameter is heavily influenced by extreme
415 values. The length of ROH tagged by the identified haplotypes for the medium-high and
416 high LD scenarios was similar across negative percentiles and QTL scenarios with a
417 median (1^{st} quartile – 3^{rd} quartile) of 12.15 (10.07-13.41). The haplotypes identified for
418 the low and low-med LD scenarios across negative percentiles and QTL tagged longer
419 ROH stretches with a median length of 15.77 (12.23-18.64). The results show how the
420 core unfavorable haplotype identified by the algorithm, which had a median length of 7.0
421 kilobases (kb) across scenarios, in reality serves as a proxy for a much larger observed
422 ROH segment. The length of unfavorable ROH that the algorithm missed was made of
423 considerably smaller ROH (median (1^{st} quartile – 3^{rd} quartile): 5.26 (4.06-5.81) Mb) and
424 was again similar across negative percentiles and scenarios. For the incorrectly identified
425 true positive ROH effects, it should be noted that the length of ROH captured by the
426 haplotype gets longer proportional to the true ROH effect. Thus, in general, falsely
427 identified ROH regions were in our analysis characterized by being locally negative
428 around the identified unfavorable haplotype. Yet as a result of being part of an extremely
429 large ROH, positive QTL effects contained in the long ROH genotype made the overall
430 effect positive.

431 The relationship of IIL with the true genetic signal, the predictive ability of ILL
432 compared to whole genome regression values and the significance of IIL or genome-wide
433 inbreeding regression coefficients are outlined in **Figure 3**. **Panel 1 of Figure 3** describes

434 the correlation between IIL with TGV, TBV, and TDD. Across all QTL scenarios, the
435 correlation increased as the LD increased for all parameters except for TDD. Averaged
436 (95% CI) across QTL scenarios the correlation between IIL and the TGV for the low and
437 high LD scenario was 0.31 (0.29-0.32) and 0.44 (0.42-0.45), respectively. The correlation
438 between IIL and TBV were similar to the correlations between IIL and TGV. The
439 average (95% CI) correlation between IIL and TDD was 0.002 (-0.01-0.01) for all
440 scenarios, which was not unexpected, given the fact that the ROH effects are a function
441 of the alternative homozygote genotypes and not heterozygous genotypes.

442 **Panel 2 and 3 of Figure 3** summarize the effectiveness of using the IIL algorithm
443 based on its predictive ability or as a tool to minimize the frequency of unfavorable
444 haplotypes in the progeny. As outlined in **Panel 2 of Figure 3**, the correlation between
445 IIL and the phenotype increased as the level of LD increased in the population. Averaged
446 (95% CI) across QTL scenarios, the prediction accuracy of IIL was 0.34 (0.32-0.36) and
447 0.49 (0.47-0.52) for the low and high LD scenarios, respectively. Similar trends of
448 increasing prediction accuracy as the LD in a population increased were seen, as
449 expected, for the whole genome prediction values and minor differences were found
450 between the prediction accuracy for EGV and EBV. Averaged (95% CI) across QTL
451 scenarios, the prediction accuracy of EGV was 0.66 (0.64-0.67) and 0.82 (0.79-0.84) for
452 the low and high LD scenarios, respectively. These results are not unexpected since the
453 algorithm only utilizes haplotypes that have an unfavorable effect contained within ROH
454 stretches and favorable haplotypes are not included in IIL. The correlations between IIL
455 and values from the whole-genome regression model are outlined in **Figure S2 Panel 1**.

Averaged (95% CI) across scenarios the correlation between IIL and EGV was 0.50 (0.49-0.50) and in general as the LD increased so did the correlation.

The last summary statistic is outlined in **Panel 3 of Figure 3** and outlines the significance of the regression coefficient based on either genome wide inbreeding metrics or IIL. Across all genome-wide inbreeding metrics the *–log p-value* was similar across all LD scenarios, and the significance increased proportionally to the number of QTL. For example, averaged (95% CI) across scenarios and genome-wide inbreeding metrics, the average *– log p-value* were 1.12 (1.01-1.23) and 1.68 (1.49-1.87) for the scenarios with 250 and 1000 QTL, respectively. The *– log p-value* for the IIL metric across all scenarios was in all cases greater and increased as the LD in the population increased. Under the high LD scenario the average (95% CI) *–log p-value* for the IIL metric across QTL scenarios was 21.24 (19.37-23.10), corresponding to a nominal p-value of $5.96e^{-10}$.

In summary, the simulation results highlight that the algorithm identified on average 41 % of the highly unfavorable (i.e. 0.05 percentile) ROH effects across the QTL scenarios and under the high LD scenario. Moreover, the unfavorable haplotypes were effective at tagging a significantly larger ROH region. Under the high LD scenario, which closely resembles most livestock situations, the ROH that the haplotype tagged had a median length of 12.1 Mb. When combining all unfavorable haplotypes based on their probability of occurring and the effect of the haplotype being in a ROH, a moderate prediction accuracy was achieved. Furthermore, the correlation between ILL and the EGV was moderate and more importantly less than unity in all cases. Therefore, a combination of ILL and a genome-wide genetic value would allow for two animals with

similar genetic values but differ in the number of unfavorable haplotypes contained within long ROH to be distinguished.

Swine Data

To determine whether similar results were found with real data and to investigate its effectiveness across multiple traits, the algorithm was tested with two swine commercial maternal lines. The significance of the regression coefficient and the predictive ability of ILL compared to genome-wide inbreeding metrics is presented in **Table 2**. Across both breeds and for the majority of traits except for NBA and TNB in LR, ILL had a prediction accuracy greater than 0. Averaged (± SD) across traits within a breed, the average prediction accuracy was 0.15 (± 0.13) and 0.20 (± 0.04) for LR and LW, respectively. Similar to the simulation, the whole genome regression based EGV resulted in higher prediction accuracies compared to ILL across all traits and breed. The prediction accuracy averaged (± SD) across traits within a breed was 0.48 (±0.10) and 0.49 (±0.17) for LR and LW, respectively. Both prediction accuracies were lower than what was achieved in the simulation, given the lower heritability for most of the traits and the simplified assumptions employed in the simulation. The correlations between IIL and values from the whole-genome regression model are outlined in the bottom of **Figure S2 Panel 2**. Averaged (± SD) across traits within a breed the correlations between the IIL and EGV were 0.31 (± 0.13) and 0.32 (± 0.06) for LR and LW, respectively. A positive correlation (Averaged ± SD: LR = 0.07 ± 0.06; LW = 0.15 ± 0.07) was estimated between ILL and EDD.

Also, outlined in **Table 2** is the *–log p-value* of the regression coefficient when genome-wide inbreeding or ILL values were included in the model. Averaged across

traits within a breed, the IIL regression coefficient resulted in a higher *–log p-value* (i.e. lower p-value) across both breeds compared to any genome-wide inbreeding metric, while the pedigree based inbreeding metric had the lowest *–log p-value*. Out of the 9 traits, the regression coefficient was trending towards significance (P-value < 0.10) for 6 and 7 out of the 9 traits for LR and LW, respectively. Alternatively, the regression coefficient for the genome-wide metrics for LR (LW), was trending toward significance for 3 (4), 2 (2) and 0 (0) of the 9 for the proportion of the genome homozygous, diagonals of **SNPRM** or pedigree-based inbreeding, respectively. Thus, in our results ILL was the parameter that more closely aligned with the identification of functional inbreeding. It should be noted that, no single parameter had a consistently higher *–log p-value* across traits so that a combination of genome-wide inbreeding metric based on genomic information and the IIL value would likely be optimal in breeding applications.

An ideogram of regions of the genome where an unfavorable haplotype was identified by the algorithm across the 9 traits for the two lines is depicted in **Figure S3** and **S4**, respectively. Regions of the genome where long unfavorable stretches of homozygosity were observed across multiple traits/line. Conversely, other regions did not appear to harbor unfavorable stretches of homozygosity. The number of regions that have an unfavorable effect across at least 4 of the 9 traits is outlined in **Table 3** and placed into categories based on the relationship between the traits. A summary of the regions and the least square mean difference between an animal in an ROH versus nonROH across both breeds is outlined in **Table S2.** A total of 4 and 13 regions were found that had at least one production and reproduction trait affected by a tag haplotype in LR and LW, respectively. A total of 3 regions across both breeds were associated only with

reproductive traits. Summary statistics on the median ROH length that the unfavorable haplotype tagged and the average frequency of the ROH genotype across traits and breeds is outlined in **Table S3**. The average median length of the unfavorable haplotype across trait and breeds was 1.56 and 1.54 Mb for LR and LW, respectively. Similarly to what found in simulated data, the unfavorable haplotype tagged a larger ROH of 9.55 and 9.12 Mb averaged across traits within LR and LW, respectively, corresponding to (averaged across traits) 172 and 156 SNP for LR and LW, respectively.

Lastly, the correlation between the diagonals and off-diagonals of **ILM** for each trait and genome-wide relationship matrices is presented in **Figure S5** and **S6** for LR and LW, respectively. As shown by the lower diagonal of each matrix, correlations between the off-diagonal elements of the ILM across all traits and genome-wide relationships are all favorably correlation. Any change in the off-diagonal **ILM** value for one trait would result in a similar (in the favorable direction) or negligible change in other traits. The average off-diagonal elements across traits for LR had an absolute correlation of 0.23, 0.28 and 0.34 for A, SNPRM and ROH5RM, respectively. Slightly lower correlations were found for LW and averaged across traits the absolute correlation was 0.14, 0.20 and 0.21 for A, SNPRM and ROH5RM, respectively. In general, the correlations between the IIL values across traits and genome-wide inbreeding metrics were similar to the off-diagonals and the majority of them were in the same direction. In some instances, the correlations between the values were antagonistic, for example LR between the SNPRM and the IIL values across all traits, although the correlations between the genome-wide inbreeding metrics were much lower compared to the off-diagonal elements.

DISCUSSION

547 The objective of this study was to implement a strategy to identify haplotypes
548 within long ROH that tag an IBD segment due to recent inbreeding. Haplotypes within
549 ROH were targeted since previous results via simulation by Keller et al. (2011) have
550 shown that ROH based genome-wide inbreeding metrics have a higher association with
551 the recessive mutation load compared to pedigree or SNP-by-SNP based inbreeding
552 metrics. The rationale behind the algorithm proposed stems from previous research
553 investigating the phenotypic effect of a region being in an ROH (Pryce et al., 2014;
554 Howard et al., 2015; Saura et al., 2015). One of the major pitfalls of previously utilized
555 methods is that they assume that any ROH genotype within a region of interest has an
556 unfavorable effect, which is most likely not the case. Instead, the unfavorable effect is
557 likely due to a single unique ROH genotype with the remaining ones resulting in no
558 unfavorable effect. Thus, the necessity of identifying unique ROH genotypes associated
559 with an unfavorable phenotype. The primary outcome of the proposed algorithm is a list
560 of unfavorable haplotypes. Multiple algorithms already exist to manage unfavorable
561 mutations or haplotypes within breeding programs so that the ones identified by the
562 algorithm could be easily incorporated into previously developed pipelines (Kinghorn,
563 2011; Cole, 2015).

564 Within the algorithm, multiple aggregation steps are implemented to confine the
565 unfavorable haplotype to the core of the observed ROH genotype in a way that is
566 consistent across individuals. As result of the aggregation step, each haplotype serves as a
567 tag for a much larger ROH segment. In this regard, the data presented confirm that the
568 aggregation steps are successful in identifying tag haplotypes contained within a much
569 larger ROH genotype. Across both swine breeds and in the simulated data set, the median

570 length of the ROH the haplotype tagged was greater than 9 Mb and the tag haplotype was
571 around 1 Mb. Furthermore, simulation results highlighted that the true ROH effects that
572 were not identified were shorter ROH (5.26 Mb) compared to the ones that were
573 identified (13.96). The ability to capture short IBD regions depends on the marker density
574 as described by Ferenčaković et al. (2013) and the marker density utilized in the current
575 study might not be sufficient to capture these short IBD regions effectively. The impact
576 of the density was not investigated here to limit the number of scenarios generated, yet its
577 impact should be considered in the future. Lastly, the simulation highlighted how in some
578 cases the algorithm incorrectly identified true positive ROH effects that were
579 characterized as being much longer compared to correctly identified negative ROH
580 effects. The distribution of the length of ROH has a heavy tail and therefore the
581 frequency of long ROH is low, but they do exist within the genome across individuals.
582 These incorrectly identified true positive ROH regions were locally negative around a tag
583 unfavorable haplotype, but being in longer than average ROH their combined effect was
584 ultimately positive.

585 We investigated the ability of the algorithm to identify unfavorable haplotypes
586 and their potential use. The frequency at which ROH occurs within the genome had a
587 large impact on the ability of the algorithm to identify unfavorable haplotypes. Medium-
588 high and high LD scenarios have LD patterns similar to those observed in livestock
589 species. Under these premises the algorithm was effective at capturing unfavorable
590 genomic regions. The proportion of highly unfavorable ROH genotypes (i.e. < 0.05
591 percentile) that the algorithm captured under the high LD scenario varied across QTL
592 scenarios. As the number of QTL increased the proportion of ROH genotypes captured

593 decreased. The average (95% CI) proportion of highly unfavorable ROH genotypes the
594 algorithm captured was 0.52 (0.42-0.62), 0.39 (0.32-0.46) and 0.33 (0.27-0.39) for the
595 scenarios with 250, 500 and 1000 QTL, respectively. The prediction accuracy based on
596 real data (average ± SD: 0.17±0.10) was roughly half of what was observed with the
597 simulated data (high LD scenario mean (95% confidence interval (CI)): 0.49 (0.47-0.52)),
598 although across the majority of traits, IIL had a prediction accuracy that was greater than
599 zero. A prediction accuracy near zero was observed in LR for NBA and TNB, which may
600 be due to multiple factors including purging of unfavorable ROH genotypes due to strong
601 selection for initial litter size within the line as well as a smaller dataset than the one used
602 in the LW population. In our study, whole genome regression based EGV resulted in a
603 moderate predictive ability (average ± SD across trait and breed: 0.48±0.14). The use of a
604 whole-genome regression method to benchmark the algorithm was used to illustrate the
605 limitations of the algorithm. The algorithm only test for regions contained in longer ROH
606 resulting in an unfavorable phenotype and should be used in conjunction with other
607 methods to increase the overall genomic variability and limit the accumulation of
608 inbreeding. Importantly, a moderate positive correlation between IIL and EGV was
609 observed in the simulated (high LD scenario mean (95% confidence interval (CI)): 0.54
610 (0.53-0.56)) and swine (average ± SD: 0.31±0.10) datasets. Thus, the combination of the
611 two metrics could allow for a breeder to more effectively manage the risks associated
612 with sire or mate selection, allowing to better evaluate the trade-off between the genetic
613 value of the progeny and undesirable side effects associated with inbreeding. Lastly, the
614 use of the algorithm along with methods to identify lethal mutations/haplotypes

615 (VanRaden et al., 2011) would allow breeders to comprehensively manage genomic
616 diversity and recessive load in a population.

617 The two maternal lines utilized in this study have been under intense selection for
618 multiple generations, which has potentially resulted in high and heterogeneous levels of
619 homozygosity across the genome. This has been investigated recently by Howard et al.
620 (2016), which estimated the proportion of the genome in a ROH of at least 5 Mb to be
621 0.17 and 0.19 for LR and LW, respectively. Furthermore, nearly all chromosomes across
622 both breeds contained regions of the genome with high levels of ROH. Under this
623 premise, it is likely that the impact of genome-level homozygosity would be regressed
624 toward zero, since homozygosity in some regions of the genome would no longer be
625 unfavorable. This result is partially verified by the ideogram outlined in **Figure S3** and
626 **S4**, whereby some regions of the genome have unfavorable haplotypes spread across
627 multiple traits and other do not have any unfavorable regions. The impact of haplotypes
628 contained within an ROH for regions that were significant across multiple traits can be
629 quite large. For example, an animal homozygous for a tag haplotype on SS9 (28.9-30.6)
630 within the LR breed would be predicted to have 1.66 fewer pigs born alive, 1.32 fewer
631 total pigs born, 4.0 % more pigs born dead and the litter would be on average 0.07 kg
632 smaller than an animal not being homozygous for the tag haplotype.

633 In general, the genetic diversity of a population is managed through the
634 relationship of the parents based on the expectation that the inbreeding in the progeny is
635 equal to half of the coancestry between the parents (Falconer and Mackay, 1996). As
636 previously discussed, since inbreeding depression is heterogeneous across the genome, a
637 measure that has a higher relationship with the genetic load of an individual may serve as

638 a better metric to manage the degree of inbreeding depression that exists within a
639 population. Therefore, linear mixed models (i.e. Model 1 described in the section
640 outlining the algorithm) that included either genome-wide inbreeding metrics or the IIL
641 value in predicting a phenotype were evaluated and the corresponding *–log p-value* was
642 estimated for each specific inbreeding regression coefficient. Across all simulated
643 scenarios and on average across both swine breeds, the significance of the regression
644 coefficient for the IIL value was higher compared to any other genome-wide metric. Yet
645 for some traits genome-wide metrics were more significant. When both the most
646 significant genome-wide inbreeding metric and ILL were included in the model, similar
647 significance values remained. This highlight how genome-wide inbreeding and ILL
648 metrics are capturing different signals. Based on our results, a combination of a genome-
649 wide relationship matrix and **ILM** could be useful in effectively manage the risks
650 associated with choosing an individual/mating combination. Future research should look
651 at the long-term benefits of including the ILM in mating designs in terms of diversity and
652 genetic load. Also, methods to incorporate multiple metrics including the genetic value,
653 genetic diversity, lethal mutations and the unfavorable haplotypes from the algorithm into
654 an index value should be developed.

655 Breeding objective are in the near totality of cases comprised of several
656 economically important traits and thus the relationship between the **ILM** across traits is
657 of importance. For the two breeds investigated the off-diagonal values across all traits
658 resulted in a favorable or negligible change across all traits. Thus, the use of the **ILM**
659 matrix for a given trait would result in a favorable increase or negligible change in the
660 phenotype of the remaining traits. Furthermore, based on genome-wide relationship

661 metrics (i.e. pedigree or genomic), the off-diagonals elements are favorably correlated
662 with off-diagonal elements of the **ILM** matrix across traits and breeds. Therefore, as one
663 changes the **ILM** values in the favorable direction, the relationship across mating pairs is
664 reduced, which is desirable and expected. Future research should investigate methods to
665 combine **ILM** across traits in the breeding objective. In general, the diagonal values had
666 similar trends as the off-diagonals across traits and relationship matrices. One of the
667 major differences between the two values related to an antagonistic relationship for LR
668 between the SNPRM and the IIL values across all traits. The inbreeding correlations had
669 a much lower correlation than off-diagonals elements and even more so within the LR
670 breed.

671 In the present study variance components were not re-estimated for each window
672 in Stage 2, which may have impacted the t-statistic. We utilized ASreml, which does re-
673 estimate the variance components for each window, to determine the sensitivity of fixing
674 variance components. The difference between the T-statistic from the algorithm and the
675 one from ASReml is outlined in **Table S4**. Across all breeds and traits, the differences
676 between the two were negligible. In addition, across all breeds and traits the T-statistic
677 from the algorithm gave a conservative estimate compared to the ones derived from
678 ASreml. The algorithm proposed may tag short haplotypes instead of long ones that
679 aren't most likely IBD segments as a result of recent inbreeding. Averaged across traits
680 the proportion of ROH genotypes that were below 1, 2 and 3 Mb with LR (LW) was 2.0
681 (1.7), 8.3 (8.4) and 16.0 (16.2) percent, respectively. The algorithm trapped short ROH
682 genotypes (albeit at a low frequency). Further improvements of the algorithm in the
683 future should focus on reducing the frequency of trapping short ROH.

Previous studies have investigated ROH effects by accounting for the additive genotypic value of the region in the model by either including SNP contained within the region investigated (Pryce et al., 2014) or using phenotypes that have been corrected for the additive effect (Howard et al., 2015). When utilizing a separate model for each window, the simulation and swine data sets have illustrated that the ROH tagging haplotype can span many Mb and is variable across animals within and across windows. Therefore, the number of SNP to include before and after the haplotype in the model to account for the additive effect for a given region is difficult to determine. More importantly, the independence between additive and dominance effects in the classical treatment (Falconer and Mackay, 1996) is to an extent a convenient artifact that allows orthogonally of the additive and dominance estimates. In reality, and as outlined in Huang & Mackay (2016), depending on the parameterization of the model the variance explained by either additive, dominance or epistasis can be rearranged and placed more heavily into any of the three categories. This is chiefly due to the fact that three effects are in real situation non-orthogonal to each other, so that the variance from a particular effect can be "consumed" by another effect. This is an important point as additive and dominance are two intrinsically inseparable terms, since if an allele is dominant over another ($a \neq 0$, $d \pm a$), there must necessarily be additive homozygous effects ($a \neq 0$; Huang and Mackay, 2016). The non-orthogonal relationship between additive and dominance effects has been confirmed with real data (Wellmann and Bennewitz, 2011; Wellmann and Bennewitz, 2012). The non-orthogonal relationship was also observed in the current simulation study. The correlation between ILL and true dominance deviation was essentially 0 across all scenarios, although a positive correlation (0.14) was observed

between ILL and the estimated dominance deviation EDD was observed. Under this premise, the ability to efficiently estimate the additive and dominance effect and their potential interactions for QTL that are at a low frequency is severely reduced. Lastly, the application of the associated haplotypes identified in mating plans when correcting for the additive effect is even more complex due to a lack of clear interpretation between the combined additive and ROH effect for a window. Therefore, in our analysis priority was given to estimating the genotypic value of ROH segments that are susceptible to displaying reduced performance based on the combined genotypic value of the given segment. Based on this premise, we make no attempt at trying to understand the number of mutations present within the ROH, the degree of epistasis that occurs or the inheritance pattern of QTL within the segment.

Conclusions

We have outlined an algorithm that identifies unfavorable haplotypes contained within an ROH that give rise to a reduced phenotype. Across simulated and real datasets the unfavorable haplotype tags a much larger ROH region that has a high probability of being IBD due to its length. Furthermore, the accuracy of prediction for the majority of the traits was greater than zero. On the real swine datasets, multiple haplotypes were identified that had a consistent unfavorable effect across multiple traits. The use of this algorithm and the associated haplotypes allow for breeding programs to more effectively identify unfavorable regions and mating programs can be used to minimize the frequency of ROH occurring in the next generation.

LITERATURE CITED

729 Charlesworth, D., and B. Charlesworth. 1987. Inbreeding Depression and its
730 Evolutionary Consequences. Annu. Rev. Ecol. Syst. 18:237-268.
731 Chen, G. K., P. Marjoram, and J. D. Wall. 2009. Fast and flexible simulation of DNA
732 sequence data. Genome Res. 19(1):136-142. doi: 10.1101/gr.083634.108.
733 Cole, J. B. 2015. A simple strategy for managing many recessive disorders in a dairy
734 cattle breeding program. Genet. Sel. Evol. 47:94. doi: 10.1186/s12711-015-0174-
735 9.
736 Falconer, D. S., and T. F. C. Mackay. 1996. Introduction to quantitative genetics. 4th
737 Edition. Longman Scientific and Technical, New York.
738 Ferenčaković, M., J. Sölkner, and I. Curik. 2013. Estimating autozygosity from high-
739 throughput information: effects of SNP density and genotyping errors. Genet. Sel.
740 Evol. 45:42. doi: 10.1186/1297-9686-45-42.
741 Garrick, D. J., J. F. Taylor, and R. L. Fernando. 2009. Deregressing estimated breeding
742 values and weighting information for genomic regression analyses. Genet. Sel.
743 Evol. 41:55. doi: 10.1186/1297-9686-41-55.
744 Gilmour, A., B. Cullis, S. Welham, B. Gogel, and R. Thompson. 2004. An efficient
745 computing strategy for prediction in mixed linear models. Comput. Stat. Data
746 Anal. 44(4):571-586. doi:10.1016/S0167-9473(02)00258-X.
747 Gilmour, A. R., B. J. Gogel, B. R. Cullis, and R. Thompson. 2009. ASReml User Guide
748 Release 3.0.
749 Henderson, C. R. 1976. A Simple Method for Computing the Inverse of a Numerator
750 Relationship Matrix Used in Prediction of Breeding Values. Biometrics. 32(1):69-
751 83. doi: 10.2307/2529339.

752 Howard, J. T., M. Haile-Mariam, J. E. Pryce, and C. Maltecca. 2015. Investigation of
753 regions impacting inbreeding depression and their association with the additive
754 genetic effect for United States and Australia Jersey dairy cattle. BMC Genomics.
755 16:813. doi: 10.1186/s12864-015-2001-7
756 Howard, J. T., F. Tiezzi, Y. Huang, K. A. Gray, and C. Maltecca. 2016. Characterization
757 and management of long runs of homozygosity in parental nucleus lines and their
758 associated crossbred progeny. Genet. Sel. Evol. 48:91. doi:10.1186/s12711-016-
759 0269-y.
760 Howard, J. T., F. Tiezzi, J. E. Pryce, and C. Maltecca. In Press. A combined coalescence
761 forward in time simulator software for pedigreed populations undergoing
762 selection for complex traits. J. Anim. Breed. Genet.
763 Huang, W., and T. F. C. Mackay. 2016. The Genetic Architecture of Quantitative Traits
764 Cannot Be Inferred from Variance Component Analysis. PLoS Genet.
765 12:e1006421. doi:10.1371/journal.pgen.1006421.
766 Keller, M. C., P. M. Visscher, and M. E. Goddard. 2011. Quantification of inbreeding
767 due to distant ancestors and its detection using dense single nucleotide
768 polymorphism data. Genetics. 189(1):237-249. doi: 10.1534/genetics.111.130922.
769 Kinghorn, B. P. 2011. An algorithm for efficient constrained mate selection. Genet. Sel.
770 Evol. 43:4. DOI: 10.1186/1297-9686-43-4.
771 Knol, E. F., B. Nielsen, and P. W. Knap. 2016. Genomic selection in commercial pig
772 breeding. Anim. Front. 6(1):15–22. doi:10.2527/af.2016-0003.

773 Legarra, A., C. Robert-Granie, E. Manfredi, and J.-M. Elsen. 2008. Performance of
774 Genomic Selection in Mice. Genetics. 180(1):611-618.
775 doi:10.1534/genetics.108.088575.
776 Lopes, M. S., J. W. M. Bastiaansen, L. Janss, E. F. Knol, and H. Bovenhuis. 2016.
777 Genomic prediction of growth in pigs based on a model including additive and
778 dominance effects. J. Anim. Breed. Genet. 133(3):180-186. doi:
779 10.1111/jbg.12195.
780 Lopes, M. S., F. F. Silva, B. Harlizius, N. Duijvesteijn, P. S. Lopes, S. E. Guimarães, and
781 E. F. Knol. 2013. Improved estimation of inbreeding and kinship in pigs using
782 optimized SNP panels. BMC Genet. 14:92. DOI: 10.1186/1471-2156-14-92.
783 Perez, P., and G. de los Campos. 2014. Genome-Wide Regression and Prediction with the
784 BGLR Statistical Package. Genetics. 198(2):483-495.
785 doi:10.1534/genetics.114.164442.
786 Pryce, J. E., M. Haile-Mariam, M. E. Goddard, and B. J. Hayes. 2014. Identification of
787 genomic regions associated with inbreeding depression in Holstein and Jersey
788 dairy cattle. Genet. Sel. Evol. 46:71. doi: 10.1186/s12711-014-0071-7.
789 Putz, A. M., F. Tiezzi, C. Maltecca, K. A. Gray, and M. T. Knauer. 2015. Variance
790 component estimates for alternative litter size traits in swine. J. Anim. Sci.
791 93(11):5153-5163. doi:10.2527/jas.2015-9416.
792 Saura, M., A. Fernández, L. Varona, A. I. Fernández, M. Á. R. de Cara, C. Barragán, and
793 B. Villanueva. 2015. Detecting inbreeding depression for reproductive traits in
794 Iberian pigs using genome-wide data. Genet. Sel. Evol. 47:1. doi:
795 10.1186/s12711-014-0081-5.

796 Simmons, M. J., and J. F. Crow. 1977. Mutations affecting fitness in Drosophila
797 populations. Annu. Rev. Genet. 11:49-78. doi:
798 10.1146/annurev.ge.11.120177.000405.
799 VanRaden, P. M. 2008. Efficient methods to compute genomic predictions. J Dairy Sci.
800 91(11):4414-4423. doi: 10.3168/jds.2007-0980.
801 VanRaden, P. M., K. M. Olson, D. J. Null, and J. L. Hutchison. 2011. Harmful recessive
802 effects on fertility detected by absence of homozygous haplotypes. J. Dairy Sci.
803 94(12):6153–6161. doi:10.3168/jds.2011-4624.
804 Welham, S., B. Cullis, B. Gogel, A. Gilmour, and R. Thompson. 2004. Prediction in
805 linear mixed models. Aust. N. Z. J. Stat. 46(3):325-347. doi:10.1111/j.1467-
806 842X.2004.00334.x.
807 Wellmann, R., and J. Bennewitz. 2011. The contribution of dominance to the
808 understanding of quantitative genetic variation. Genet. Res. Camb. 93(2):139-154.
809 doi: 10.1017/S0016672310000649.
810 Wellmann, R., and J. Bennewitz. 2012. Bayesian models with dominance effects for
811 genomic evaluation of quantitative traits. Genet. Res. Camb. 94(1):21-37. doi:
812 10.1017/S0016672312000018.
813 Wolc, A., C. Stricker, J. Arango, P. Settar, J. E. Fulton, N. P. O'Sullivan, R. Preisinger,
814 D. Habier, R. Fernando, D. J. Garrick, S. J. Lamont, and J. C. Dekkers. 2011.
815 Breeding value prediction for production traits in layer chickens using pedigree or
816 genomic relationships in a reduced animal model. Genet. Sel. Evol. 43:5.
817 doi:10.1186/1297-9686-43-5.

818 Xiang, T., O. F. Christensen, Z. G. Vitezica, and A. Legarra. 2016. Genomic evaluation
819 by including dominance effects and inbreeding depression for purebred and
820 crossbred performance with an application in pigs. Genet. Sel. Evol. 48(1):92.
821 doi: 10.1186/s12711-016-0271-4.

822
823
824
825
826
827
828
829
830
831
832
833
834
835
836
837
838
839

Table 1. The model utilized, estimated genetic parameters and the number of animals across traits for the Landrace (LR) and Large White (LW) population.

Breed	Trait[1]	Fixed Effects[1]	Genetic Parameters[2]		Animals (Records)	
			h^2	r^2	Training	Validation
LR	NBA	Parity, CG	0.082	0.149	4,005 (9,416)	1,005 (1,639)
	TNB	Parity, CG	0.082	0.149	4,003 (9,302)	998 (1,621)
	PD	Parity, CG	0.085	0.156	4,003 (9,293)	998 (1,621)
	LBW	Parity, CG, NBA	0.231	0.284	3,985 (8,648)	988 (1,586)
	PWM	Parity, CG, Pig24hrs	0.115	0.131	3,504 (6,724)	870 (1,330)
	NW	Parity, CG, Pig24hrs	0.102	0.120	3,465 (6,600)	845 (1,280)
	NWBW	Parity, CG, Pig24hrs, NW	0.144	0.211	3,465 (6,600)	845 (1,280)
	Weight	CG, Sex, Age	0.271	-	4,386 (4,386)	993 (993)
	ADG	CG, Sex, Age	0.271	-	4,386 (4,386)	993 (993)
LW	NBA	Parity, CG	0.115	0.150	5,518 (15,014)	1,232 (2,271)
	TNB	Parity, CG	0.098	0.142	5,513 (14,673)	1,228 (2,262)
	PD	Parity, CG	0.086	0.133	5,513 (14,664)	1,228 (2,262)
	LBW	Parity, CG, NBA	0.241	0.307	5,487 (13,581)	1,188 (2,155)
	PWM	Parity, CG, Pig24hrs	0.074	0.168	4,966 (10,464)	1,102 (1,824)
	NW	Parity, CG, Pig24hrs	0.053	0.115	4,901 (10,259)	1,054 (1,716)
	NWBW	Parity, CG, Pig24hrs, NW	0.144	0.203	4,901 (10,259)	1,054 (1,716)
	Weight	CG, Sex, Age	0.292	-	5,576 (5,576)	1,197 (1,197)
	ADG	CG, Sex, Age	0.291	-	5,576 (5,576)	1,197 (1,197)

[1] NBA = number born alive; TNB = total number born; PD = proportion born dead; LBW = average litter birth weight; PWM = pre-weaning mortality; NW = number weaned; NWBW = average litter wean weight; Weight = weight at off-test; ADG = average daily body weight gain from birth to off-test; CG = contemporary group based on farm, year and season; Pig24hrs = pigs in the litter after the 24 hour cutoff; Age refers to off-test age.

[2] h^2 refers to the narrow sense heritability; r^2 refers to the repeatability.

Table 2. The significance of inbreeding regression coefficient across multiple inbreeding metrics and the prediction accuracy of the individual inbreeding load (IIL) and estimated genetic value (EGV) from whole genome Bayesian Ridge Regression across traits for Landrace (LR) and Large White (LW) populations.

Breed	Trait[1]	Regression on Adjusted Phenotype –log(P-value)[2]				Prediction Accuracy	
		Pedigree Inbreeding	Genomic Inbreeding	Proportion Homozygous	IIL	EGV	IIL
LR	NBA	0.66	0.49	0.69	0.00	0.44	-0.05
	TNB	0.87	0.68	0.23	0.53	0.42	-0.09
	PD	0.15	0.00	1.42	1.94	0.53	0.15
	LBW	0.45	2.24	1.34	15.24	0.65	0.33
	PWM	0.29	1.54	0.8	2.94	0.40	0.17
	WN	0.21	1.01	0.49	4.00	0.42	0.22
	WNBW	2.14	0.66	4.36	2.51	0.64	0.22
	Weight	0.53	4.52	2.93	3.24	0.40	0.17
	ADG	0.58	4.54	2.84	4.00	0.39	0.18
	Average	0.65	1.74	1.68	3.82	0.48	0.15
LW	NBA	0.62	0.15	0.12	4.14	0.45	0.24
	TNB	0.98	0.40	0.21	2.56	0.42	0.19
	PD	0.54	1.35	1.97	1.94	0.38	0.13
	LBW	2.18	1.11	4.07	10.25	0.77	0.24
	PWM	2.11	0.33	1.37	2.09	0.36	0.18
	WN	1.71	0.12	0.00	2.91	0.29	0.25
	WNBW	0.00	0.78	2.56	3.46	0.79	0.17
	Weight	0.69	5.70	6.14	5.99	0.48	0.18
	ADG	0.73	5.76	6.09	4.77	0.48	0.17
	Average	1.06	1.74	2.50	4.23	0.49	0.20

[1] NBA = number born alive; TNB = total number born; PD = proportion born dead; LBW = average litter birth weight (LBW); PWM = pre-weaning mortality; NW = number weaned; NWBW = average litter wean weight; Weight = weight at off-test; ADG = average daily body weight gain from birth to off-test.

[2] As a reference a p-value of 0.10, 0.05 and 0.01 is equivalent to a negative log p-value of 2.30, 3.0 and 4.6, respectively.

Table 3. Summary of the number of haplotypes that displayed unfavorable effects across multiple (i.e. > 4) traits for Landrace (LR) and Large White (LW) populations.

Breed	Type of Trait[1]	Number of Haplotypes
LR	Production and Reproduction	4
	Reproduction	3
LW	Production and Reproduction	13
	Reproduction	3

[1] The type of trait refers a Production trait (i.e. weight at off-test; average daily body weight gain from birth to off-test) or a Reproductive Trait (i.e. number born alive; total number born; proportion born dead; average litter birth weight; pre-weaning mortality; number weaned; average litter wean weight).

880 **Figure 1.** Overview of algorithm that identifies unfavorable haplotypes.

881 **Figure 2.** Summary[1] of the proportion of runs of homozygosity (ROH) of at least 1
882 Megabase the algorithm captures (Panel 1) and the length of the ROH the haplotype tags
883 (Panel 2) across simulation scenarios[2] by percentile class[3] and whether the algorithm
884 identified the haplotype.

885 [1] The summary statistic in Panel 1 is the mean ± 95 % confidence interval and in Panel 2
886 is the 1st, 2nd and 3rd quartiles.

887 [2] Refers to ancestral population scenario simulated. Scenario 1 = "Ne1000" parameter in
888 Geno-Diver; Scenario 2 = "Ne250" parameter in Geno-Diver. Scenario 3 =
889 "Ne100_Scen1" parameter in Geno-Diver. Scenario 4 = "Ne70" parameter in Geno-
890 Diver.

891 [3] The ROH percentile class is outlined on the x-axis and the first 4 represent quantiles for
892 the true negative effects (i.e. 0.05 represents the highly negative ROH effects) and the
893 last 4 represent quantiles for the true positive effects (i.e. 0.95 represent highly positive
894 effects). The y-axis refers to the algorithms summary statistics for the number of true
895 ROH identified out of all true ROH effects within the given quintile.

896 [4] The number below either negative or positive ROH refers to the percentage of the ROH
897 that the algorithm correctly found out of the all negative or positive true ROH effects.

898 **Figure 3.** Summary (mean ± CI)[1] of the correlation between individual inbreeding load
899 (IIL) and the true genetic signal (Panel 1)[2], prediction accuracy for IIL and genotypic
900 estimates Bayesian ridge regression (Panel 2)[3] and significance of the regression
901 coefficient based on either a genome wide inbreeding metrics or IIL (Panel 3)[4] across
902 simulation scenarios[5].

903 [1] CI: 95% confidence interval.

904 [2] TGV: true genotypic value; TBV: true additive genetic value; TDD: true dominance

905 deviation.

906 [3] EGV: estimated genotypic value; EBV: estimated breeding value.

907 [4] Pedigree: pedigree inbreeding; Genomic: genomic inbreeding based on diagonals of

908 genomic relationship matrix; Homozygosity: proportion of genome homozygous.

909 [5] Refers to ancestral population scenario simulated. Scenario 1 = “Ne1000” parameter in

910 Geno-Diver; Scenario 2 = “Ne250” parameter in Geno-Diver. Scenario 3 =

911 “Ne100_Scen1” parameter in Geno-Diver. Scenario 4 = “Ne70” parameter in Geno-

912 Diver.

913 **Figure 1.** Overview of algorithm that identifies unfavorable haplotypes.

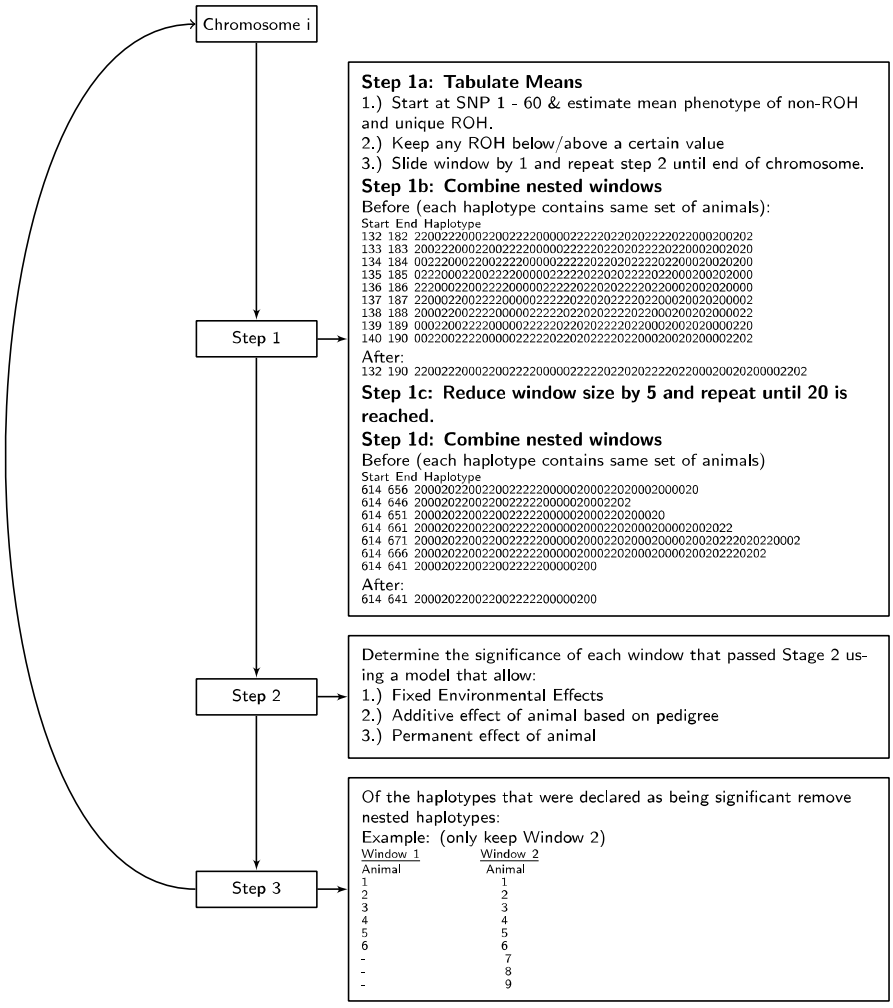

914

Figure 2. Summary[1] of the proportion of runs of homozygosity (ROH) of at least 1 Megabase the algorithm captures (Panel 1) and the length of the ROH the haplotype tags (Panel 2) across simulation scenarios[2] by percentile class[3] and whether the algorithm identified the haplotype.

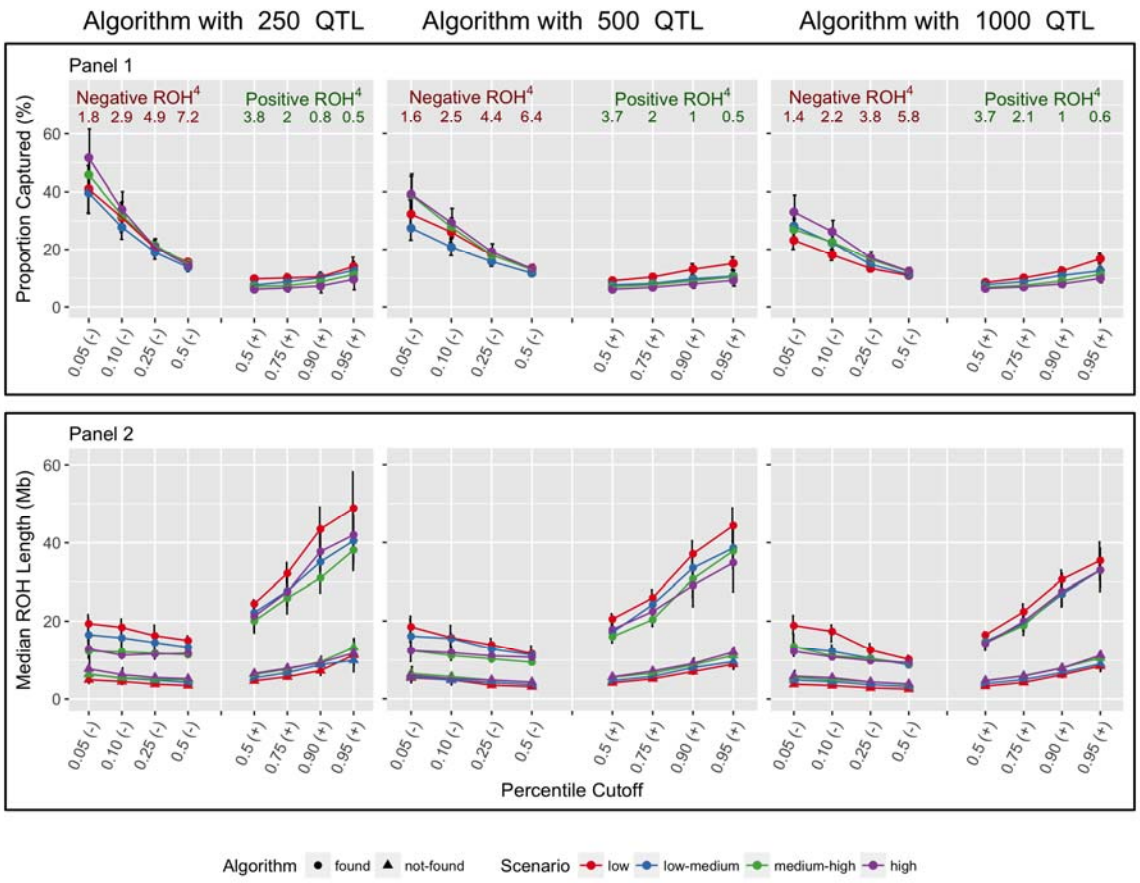

Figure 3. Summary (mean ± CI)[1] of the correlation between individual inbreeding load (IIL) and the true genetic signal (Panel 1)[2], prediction accuracy for IIL and genotypic estimates Bayesian ridge regression (Panel 2)[3] and significance of the regression coefficient based on either a genome wide inbreeding metrics or IIL (Panel 3)[4] across simulation scenarios[5].